Y. Suzuki et al.

Impact of nonlinear 3D equilibrium response on edge topology and divertor heat load in Wendelstein 7-X

Preprint of Paper to be submitted for publication in
Plasma Physics and Controlled Fusion

Impact of nonlinear 3D equilibrium response on edge topology and divertor heat load in Wendelstein 7-X

Y. Suzuki[1,2] and J. Geiger[3]

[1] National Institute for Fusion Science, 509-5292 Toki, Japan
[2] SOKENDAI, The Graduate University for Advanced Studies, 509-5292 Toki, Japan
[3] Max-Planck-Institut fuer Plasmaphysik, D-17491 Greifswald, Germany

E-mail: suzuki.yasuhiro@LHD.nifs.ac.jp

Abstract. The impact of the three-dimensional equilibrium response on the plasma edge topology is studied. In Wendelstein 7-X, the island divertor concept is used to assess scenarios for quasi-steady-state operation. However, the boundary islands necessary for the island divertor are strongly susceptible to plasma beta and toroidal current density effects because of the low magnetic shear. The edge magnetic topology for quasi-steady-state operation scenarios is calculated with the HINT-code to study the accompanying changes of the magnetic field structures. Two magnetic configurations have been selected which had been investigated in self consistent neoclassical transport simulations for low bootstrap current but which use the alternative natural island chains to the standard iota value of 1 ($\iota_b = 5/5$, periodicity), namely, at high-iota ($\iota_b = 5/4$) and at low-iota ($\iota_b = 5/6$). For the high-iota configuration, the boundary islands are robust but the stochasticity around them is enhanced with beta. The addition of toroidal current densities enhances the stochasticity further. The increased stochasticity changes the footprints on in-vessel components with a direct impact on the corresponding heat loads. In the low-iota configuration the boundary islands used for the island divertor are dislocated radially due to the low shear and show even healing effects, i.e. the island width vanishes. In the latter case the plasma changes from divertor to limiter operation. To realize the predicted high-performance quasi-steady-state operation of the transport simulations, further adjustments of the magnetic configuration may be necessary to achieve a proper divertor compatibility of the scenarios.

1. Introduction

Wendelstein 7-X (W7-X) is a five period advanced stellarator with major radius of 5.5m and a minor radius of about 0.5m whose magnetic configuration has been optimized for good MHD-equilibrium and -stability and good neoclassical confinement [1, 2]. The main mission of W7-X is to show the reactor viability of such types of configurations by demonstrating quasi-steady-state operation with high performance plasmas, i.e. high $nT\tau$ with 10 MW ECRH-power at the nominal field of 2.5T and pulse durations of up to 30 min). For quasi-steady-state operation, control of particle and energy exhaust is a key issue. In W7-X, the island divertor concept has been adopted for this purpose [3]. In stellarator and heliotron devices, the helical divertor is an obvious approach [4], because the separatrix corresponding to the polar number of the helical winding law, L, appears naturally. This separatrix can be used to divert the particle and energy fluxes and form a private flux region. However, advanced stellarators are designed by three-dimensionally (3D) shaping their plasma boundary to optimize the desired target properties for which a Fourier representation of the plasma boundary is generally used. This means that the separatrix structure for a divertor configuration cannot be directly be accessed. The low-shear approach the to advanced stellarator design tries to avoid low order rational surfaces in the iota-profile for reasons of stability and to avoid island formation in the confinement volume with a possible degradation of the magnetic configuration and of the plasma confinement. However, if rational surfaces are present, magnetic islands are easily generated with rather small magnetic field components ($B^r/B \sim 10^{-4}$). Putting a low order rational surface at the boundary, the naturally appearing islands form a separatrix which can be utilized to divert particle and energy fluxes. Figure 1 shows the vacuum magnetic field for the standard configuration of W7-X. Puncture plots of three poloidal cross sections are shown corresponding to the bean-shaped, the tear-drop (mid-half-period) and triangular (half-period) cross sections. In those plots, red dots, green dots, and blue dots indicate the diverted plasma, boundary islands, and the scrape-off layer (SOL), respectively. For the standard configuration, the rotational transform, ι, at the plasma boundary is one. Due to the five-fold periodicity, the 5/5 islands appearing at the plasma boundary are distinct, i.e. are not connected with each other. Purple lines in figure 1 indicate in-vessel components consisting of divertor and baffle plates. For this configuration the main interaction region are the horizontal divertor plates intersecting the upper and lower O-points of 5/5 islands in the bean-shaped cross section. For stable divertor operation, a stable boundary topology of the magnetic configuration with respect to the divertor modules is necessary. The small magnetic shear of the W7-X configurations leaves the rotational transform profiles highly susceptible to changes due to plasma beta effects or due to toroidal current densities in the 3D MHD equilibrium, i.e. the '*nonlinear 3D equilibrium response*. Although these effects have been diminished by the optimization of W7-X, they still exist and need to be considered in investigations of appropriate divertor operation scenarios.

Previous 3D MHD equilibrium studies did not include toroidal current densities [5,

6, 7, 8, 9]. For example, Drevlak *et al* [7] studied the 3D MHD equilibrium for a large volume configuration with 5/5 boundary islands and found a significant shrinkage of the plasma volume due to due to the non-linear 3D equilibrium response. While the position of the boundary islands was robust the size of the good island surfaces decreased and the stochasticity around them increased. Suzuki *et al* studied different configurations with different boundary iotas [8, 9]. For a low-iota configuration, self-healing of boundary islands was found. When increasing the plasma beta the boundary island width shrank, disappeared at a certain beta-value and then reappeared with the opposite island phase, i.e. o- and x-point locations had changed position. In such a case the plasma boundary transport scenario changes from divertor to limiter and back to divertor operation depending on the achieved beta-values due to the non-linear 3D equilibrium response. On the other hands, Geiger *et al* studied the effects of net toroidal current densities on the boundary islands using the VMEC/EXTENDER approach [10] and also found the self-healing of the boundary islands due to the plasma beta. It was also pointed out that net toroidal current densities should be considered when searching for appropriate island divertor operation scenarios. However, the VMEC/EXTENDER approach [7] suffers from an inconsistency between the magnetic topology and the internal equilibrium profiles since, VMEC assumes nested flux surfaces and internal profiles are not flattened when islands or stochastic regions appear. It should perhaps be mentioned that in addition to the "self-healing" found by MHD codes, there are non-MHD mechanisms that cause self-healing of islands in the core of the plasma [14]

In this study we investigate the two boundary island topologies alternative to the 5/5-island chain whose boundary is determined by the corresponding low order rational values below and above $\iota_b = 1$, i.e. a low-iota (5/6) and a high-iota (5/4) configuration. The configurations had been investigated in a cycle of equilibrium calculations and neoclassical transport simulations to achieve a self-consistent core-plasma scenario for a high-performance quasi-steady-state operation [12]. To have a conservative scenario, the coil currents of W7-X had been fine-tuned to achieve small bootstrap currents in these scenarios. The resulting pressure and current profiles are used to study their impact on the self-consistent equilibrium fields calculated with the HINT-code which is free from the assumption of nested flux surfaces. The paper is organized as follows: in the next section, the chosen magnetic configurations and the scenarios are discussed. In section. 3, the edge magnetic topology and its impact on the heat load on in-vessel components is discussed. In particular, the change of the edge magnetic topology due to the non-linear 3D equilibrium response is emphasized. The last section summarizes the results.

2. High-performance steady state operation scenarios

As earlier mentioned magnetic configurations with a small bootstrap current are ideal candidates for high-performance, quasi-steady-state plasmas allowing a stable boundary topology for which proper divertor operation can be expected. To realize

high-performance plasmas in W7-X in quasi-steady-state operation relies on high-density ($1.5 \times 10^{20} m^{-3}$ or larger) and on the cw-140GHz-ECRH system which needs to be operated in O2-mode at high density instead of X2-mode for densities below $1.2 \times 10^{20} m^{-3}$ (X2-mode cut-off). This base scenario was investigated in [12] with respect to the core confinement and the resulting bootstrap current for the three boundary iota values at W7-X offering a divertor topology, i.e. boundary iota values of 5/6, 5/5 and 5/4. To arrive at consistent scenarios, iterations were performed between equilibrium calculations with VMEC, calculations of the mono-energetic neoclassical transport coefficients with DKES to include the changed equilibrium properties, and transport simulations based on neoclassical transport plus a heuristic turbulent contribution, from which new profiles resulted for the pressure and the bootstrap current entering the next iteration step. The investigation showed that two configuration parameters are highly relevant for the value of the bootstrap current, namely, the strength of the toroidal mirror field (usually large field strength in the bean-shaped plane at $\varphi = 0°$, lower in the triangular one at $\varphi = 36°$) and the iota-value. For the standard iota-value of 1, a mirror field of about 11% is necessary to suppress the bootstrap current in the above high-performance scenario (B varies by $\pm 11\%$ along the magnetic axis). For the high- and low-iota configuration the different mirror fields are required, only 4% for high-iota, but 24% for low-iota.

For technical simplicity, the high performance scenarios described in [12] have been chosen with a constant magnetic field strength adjusted to a value such that at high density, i.e. at the highest beta-value in the scenario, the O2-heating is on-axis to assure high temperatures for good absorption of the ECRH. Thus, plasma start-up which is performed with X2-mode will be an off-axis heating-scheme which will gradually move towards on-axis as density and beta increases. However, at medium densities of about $0.7 - 0.8 \times 10^{20} m^{-3}$, when the heating scheme switches polarization from X2 to O2, the heating is still off-axis.In figure 2, the profiles of pressure and toroidal current density for the different stages in the scenarios for the high-iota and low-iota configurations are shown. The left column shows the profiles for the high-iota configuration and the right column for the low-iota configuration. The upper row shows the pressure profiles and the bottom row the toroidal current density profiles. For the high-iota configuration, the medium and the high density stage are plotted while for the low-iota case all three stages are shown. The pressure profile of low and medium density stages are broad due to the off-axis heating and show a peaked form for high-density when on-axis heating is realized. The total toroidal currents in the high-iota configuration is at high density only $1kA$ which results from a cancellation of positive and negative current density parts in radially different regions. A similar behaviour is seen for the low-iota configuration at high density. Here a toroidal current of about 6kA was reached. However, during the low density (start-up) phase, a stronger current density appears peaked in the pressure gradient region due to the bootstrap current driven locally around this radial location by the temperature gradients from off-axis heating. Such a localized current density is expected to result in a correspondingly more localized deviation of the iota-profile

and needs to be considered in equilibrium calculations. At higher densities the current densities are smaller, the total current stays small and the deviations of iota are expected to be smoother.

3. Impacts of 3D equilibrium response on edge magnetic topology

In this section, the impact of the plasma beta effect and the internal toroidal current density on the edge magnetic topology is discussed. The plasma is assumed to be in steady state and the magnetic field is calculated by the fully 3D equilibrium code HINT. The focus is on interactions of the edge magnetic topology and the in-vessel components.

3.1. High-iota configuration

In figure 3, Poincaré plots of the high-iota configuration for the vacuum field are shown. Three poloidal cross section corresponding to the bean-shaped, tear-drop, and triangular cross section are plotted. In the figures, in-vessel components, such as divertor and baffle plates, have also been drawn to show the interactions with the edge magnetic topology. For the high-iota configuration, the boundary iota ι_b is 5/4 and the 5/4 islands are used for divertor interaction (see figure 3(a) and (b)). As mentioned in the introduction, high-iota configurations had studied previously in [6, 8]. High-iota configurations are strongly elongated in the bean-shaped plane. Due to their phasing the boundary islands are position such that the o-point in the bean-shaped plane is at the horizontal divertor plate and the x-points show a sufficient radial distance to the divertor. However, in the tear-drop section, the inner x-point of the upper island is rather close to the vertical divertor structures (target and baffle plates). If the edge magnetic topology changes due to the non-linear 3D equilibrium response, heat loads on these in-vessel components may change significantly.

To investigate this question, a 3D equilibrium analysis has been performed using the pressure and toroidal current density shown in figure 2. In the β-sequence, the 5/4 islands show a robust behaviour up to $\beta \sim 3\%$ (high density case). However, the edge magnetic topology does change significantly. In particular, the stochasticity at the separatrix of the 5/4 islands is enhanced by the β effect and the plasma volume shrinks, which is consistent with previous studies [6, 8]. Figure 4 compares the Poincaré plots in the bean-shaped cross section of the vacuum field (a) with the 3D equilibrium fields calculated for the medium density case without and with toroidal current density, (b) and (c) respectively. For the plasma beta effect only (figure 4 (b)), higher-order rational islands (e.g. 15/13) appear and the ones further out overlap and increase the stochastic region. However, inclusion of the toroidal current density (figure 4 (c)) leads to a shrinking of the size of the islands at the boundary but the stochasticity around the high-order rationals is enhanced. To see the enhanced stochasticity more clearly, contours of the connection length, L_C, of magnetic field lines corresponding to figure 4 are shown in figure 5. L_C was calculated up to 1000 m, i.e. field lines with values larger

than 1000 m are assumed to be closed field lines. For the vacuum field, almost all field lines hitting the divertor plate are closed. However, for the 3D equilibrium fields the magnetic field lines along the separatrix of the 5/4 islands open up which means that plasma beta and toroidal current densities have a significant effect on the edge magnetic topology.

A change in the edge magnetic topology is likely to affect the heat load distribution on the in-vessel components. The enhanced stochasticity drives the radial deviation of magnetic field lines with accompanying changes of their footprints on the divertor and baffle plates. In figure 6, the footprints of the magnetic field lines on the in-vessel components are shown in a top view on one segment of the lower divertor. The bottom in the figure corresponds to the bean shape cross section and the upper part to the tear-drop cross section. For this high-iota configuration, the boundary islands is very close to the in-vessel components around toroidal location of the tear-drop cross section. The footprints with the long connection lengths start at the middle of the figures (figure 6 (a)) in the upper part. This is the so-called high-iota tail of the divertor since it preferentially sees load in high-iota configurations but less in the standard-iota and low-iota configurations. Including the plasma beta effect only (figure 6 (b)), the connection lengths of the magnetic field lines decrease in this part and the footprint pattern significantly changes. Adding further the toroidal current density (figure 6 (c)), the footprint pattern partly recovers the distribution of the vacuum case because the toroidal current density decreases the stochasticity on the high-order rational surfaces. However, an additional spot with high L_C-values appears at the edge of in-vessel components, which could be critical at this location corresponding to the less cooled baffles (on closer inspection the beta-only case already shows the onset of this heat load increase). The total bootstrap current is very small (only 1kA) but the impact of the edge magnetic topology is surprisingly large. In future scenario developments, such effects must be kept in mind.

3.2. Low-iota configuration

Figure 7 shows Poincaré plots of the vacuum field of the low-iota configuration in the same cross section as in figure 3. Previous studies of the 3D MHD equilibrium used the reference low-iota configuration [8, 9] and showed that self-healing of the 5/6 boundary islands due to finite β can be observed. The low-iota configuration in this study is somewhat distinct with respect to the toroidal mirror field present in the configuration. The reference low-iota configuration has only a mirror field of about 3.5%, while, as mentioned earlier, the mirror field here is about 24% in order to achieve a small bootstrap current. This leads to a strong toroidal variation of the cross sectional area of a flux surface. In the bean-shaped plane, where the field strength is large, the cross section is small and the islands do not intersect the divertor. As the cross sectional area of the flux surface grows when advancing toroidally, the boundary islands intersect with the vertical target and baffle plates and the plasma divertor interaction is more around the tear-

drop plane. Geiger *et al* studied this case in a self-consistent core-equilibrium/transport simulation but omitted a detailed investigation of the divertor compatibility, which is done here in a first step. For this study, the configuration used in [12], which proved to be a limiter configuration (the 5/6 islands were located slightly outside the flux surface intersecting the divertor), was adjusted to a slightly higher iota-value in order to produce a proper divertor configuration with respect to the vacuum field. In order to judge whether further adjustments for the divertor compatibility are necessary, the impact of the plasma beta effect and the toroidal current density are studied here.

Figure 8 shows the β-sequence in the tear-drop cross section, where the plasma is closest to the divertor. Contrary to the 5/4 islands of the high-iota configuration, which showed robust behaviour up to $\beta \sim 3\%$, the 5/6 islands exhibit self-healing with increasing β also in the configuration with a very large mirror field. For the low and medium density cases (figure 8 (a) and (b)), the 5/6 islands are still robust although the location of the 5/6 rational moves slightly radially outward, because the iota-profile is slightly decreased due to finite β. This again leads to a limiter-type plasma configuration where the plasma is attached to a baffle plate at the inboard side. For the high-density case with a further increase in β ($\sim 3.3\%$), the 5/6 islands are almost healed or are at the verge of switching to the opposite island phase. With a further decrease of the iota-profile due to β the resonance is further out and good flux surfaces limit the plasma in the tear-drop cross section. In addition, a higher order island (10/13) appears in the core. In figure 9 the Poincaré plots are shown for the same β-sequence as in figure 8 but now including the toroidal current density. For the low-density case, the change is drastic since the bootstrap current density flowing around the mid minor radius leads to a shift of the 5/6-island chain further inwards and a small-shear region just beyond it to the appearance of a 10/12 island chain. Such a magnetic configuration situation would be expected to generate difficulties in the start-up phase if one would try to realize this steady-state solution. In case of a more rapid build-up of density and β the self-shielding on the resistive skin-time of the plasma might allow access to medium density and β. For the medium- and high-density cases, the bootstrap current is smaller but a toroidal current density still remains. As the total bootstrap current increases iota the locations of 5/6 islands move radially inward compared to the β-only cases and moves the 5/6-islands again in reach of the divertor plates. With the profiles used here, the plasma still attaches to the baffle plate. Thus, the low-iota configuration seems to be the most sensitive one with respect to effects by plasma β and toroidal current. For a stable divertor operation, further fine-tuning of the boundary-iota and/or of the experimental scenario seems necessary. However, this is beyond the scope of the present paper.

4. Summary

The impact of the non-linear 3D equilibrium response on the edge magnetic topology has been studied by non-linear 3D MHD equilibrium calculations. Two magnetic configurations, which have been proposed for high-performance quasi-steady-state

operation scenarios with high and low boundary iotas, were considered. For the high-iota configuration, the boundary islands connected with $\iota_b=5/4$ are robust but the stochasticity around the separatrix of 5/4-islands is significantly enhanced with increasing β and with toroidal current density. The enhanced stochasticity is likely to affect the footprint patterns on the divertor and baffle plates, and new heat load location can occur on the less well cooled baffle structures. A more accurate assessment would require the use of an edge-plasma transport code, such as EMC3 [13]. For the low-iota configuration, the boundary islands due to $\iota_b=5/6$ change their radial location but can also be healed with increasing β. The toroidal current density distribution , which leads to a small, but iota-increasing total current, can help to reach a divertor configuration although more fine-tuning is still necessary. The question of a start-up scenario for the low-iota configuration is still open due to its sensitivity (very low-shear!) on β and the toroidal current densities. It should be kept in mind that for this configuration the plasma may easily change from a divertor to a limiter configuration.

As a further option, the compensation of the bootstrap current by ECCD is possible under the condition that X2-mode heating is used and the density is kept moderate (up to about $0.7 \times 10^{19} m^{-3}$). The toroidal current, I_ϕ, can then be kept small although the toroidal current density, j_ϕ, is nonzero, leading to a highly distorted internal iota-profile as discussed in [12]. Nevertheless, on the basis of this study, one might expect the edge magnetic topology to be sensitive to the internal toroidal current density distribution in the ECCD compensation case, which should be investigated in further studies.

Acknowledgments

References

[1] Grieger G *et al* 1992 *Phys. Fluids B* **4** 2081
[2] Lotz W, Nuehrenberg J and Schwab C 1991 *13th Int. Conf. on Plasma Physics Controlled Nuclear Fusion Research (Washington, DC, 1990)* vol 2 (Vienna: IAEA) p 603 (www-naweb.iaea.org/napc/physics/FEC/STIPUB844 VOL2.pdf)
[3] Renner H *et al* 2000 *Nucl. Fusion* **40** 1083
[4] Ohyabu N *et al* 1992 *J. Nucl. Mat.* **196198** 276
[5] Strumberger E 1998 *Contrib. Plasma Phys.* **38** 106
[6] Strumberger E 1997 *Nucl. Fusion* **37** 19
[7] Drevlak M *et al* 2005 *Nucl. Fusion* **45** 731
[8] Suzuki Y *et al 33rd EPS Conference on Plasma Physics* (2006) P2.119
[9] Suzuki Y *et al* 2010 *Contrib. Plasma Phys.* **50** 576
[10] Geiger J *et al Joint 19th ISHW and 16th IEA-RFP workshop* (2013) D5
[11] Suzuki Y *et al* 2006 *Nucl. Fusion* **46** L19
[12] Geiger J *et al* 2015 *Plasma Phys. Control. Fusion* **57** 014004
[13] Feng Y J *et al* 2014 *Contrib. Plasma Phys.* **54** 426
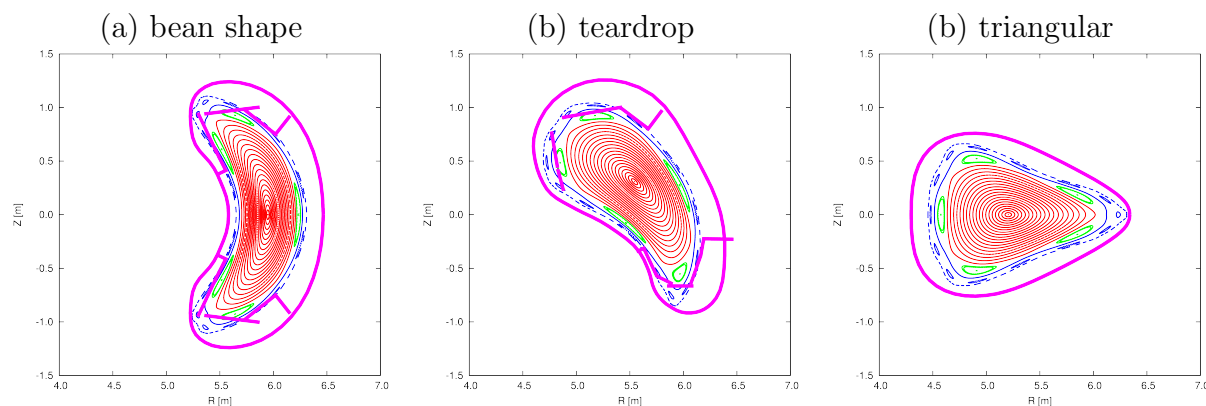[14] Hegna C C 2011 *Nucl. Fusion* **51** 113017

Figure 1. Poincaré plots of the standard configuration are shown for the vacuum field. Three poloidal cross section at the bean shape, teardrop, and triangular cross sections are plotted, respectively. Red dots, green dots, and blue dots indicate the diverted plasma, boundary islands, and the scrape-off layer (SOL), respectively. Purple lines indicate in-vessel components of divertor and baffle plates.
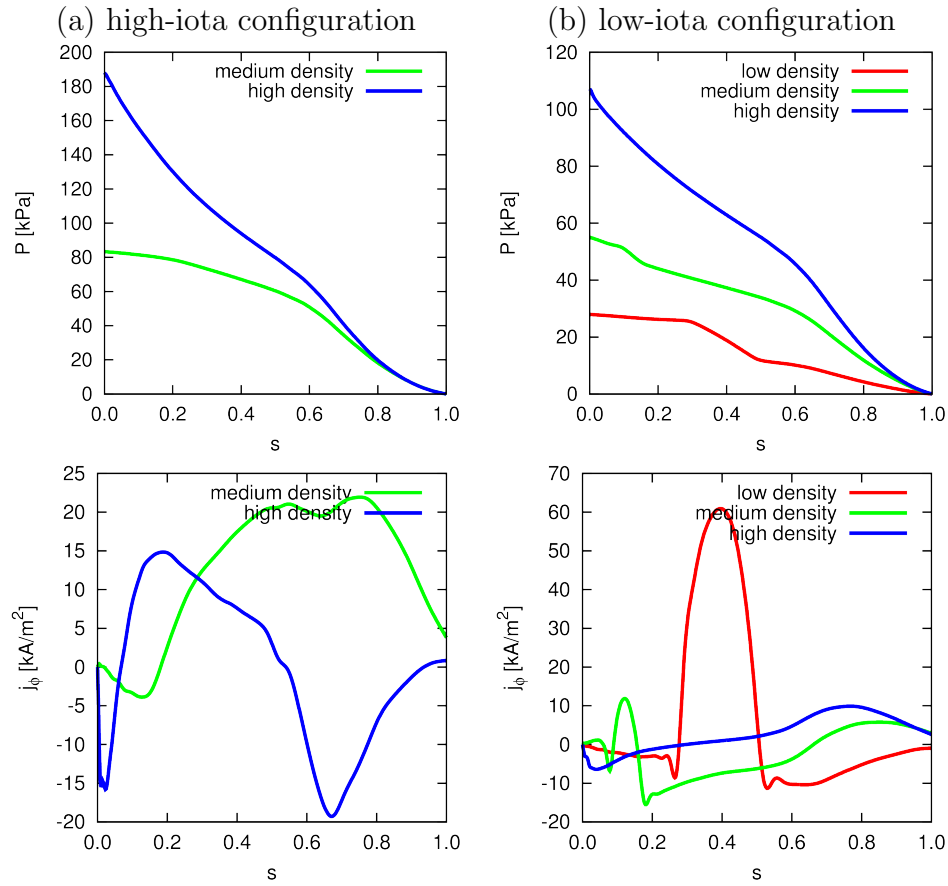
Figure 2. Profiles of the plasma pressure and toroidal current density are shown the high-iota and low-iota configurations. The left column shows the high-iota configuration and the right columns shows the low-iota configuration. The upper row shows the plasma pressure and the bottom row shows the toroidal current density.
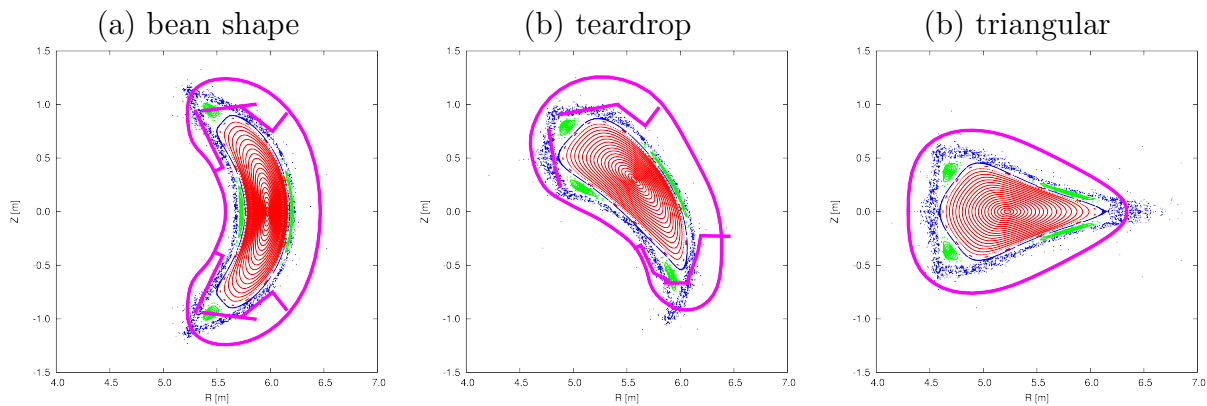

Figure 3. Poincaré plots of the standard configuration are shown for the vacuum field. The boundary iota is 5/4. Three poloidal cross section are plotted corresponding to figure 1.
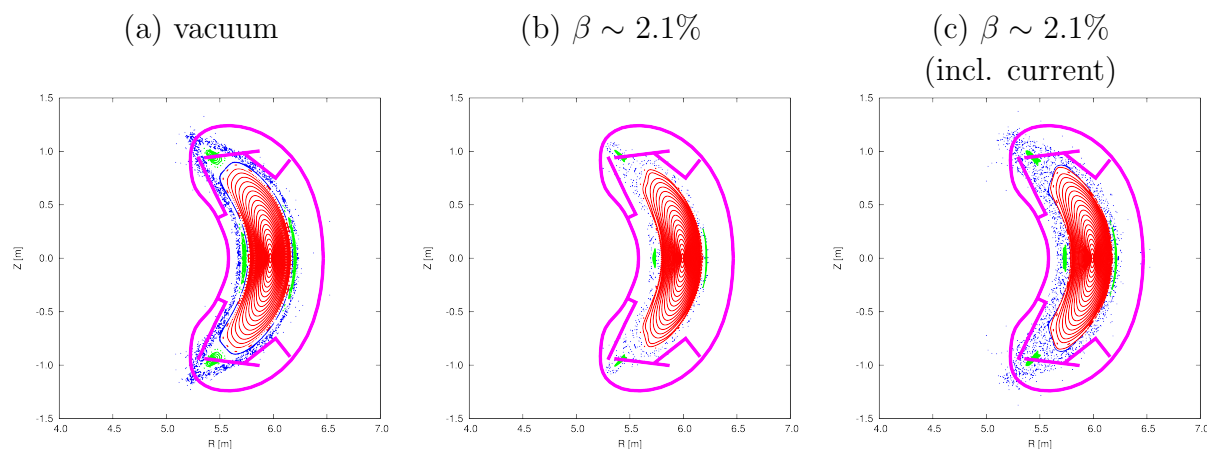
(a) vacuum   (b) $\beta \sim 2.1\%$ (c) $\beta \sim 2.1\%$
                                                    (incl. current)

Figure 4. 3D MHD equilibria for the medium density case are shown. Results are shown for a case of the beta effect only and another case including both effects of the plasma beta and toroidal current. For a comparison, the vacuum field is also shown. Red dots, green dots, and blue dots indicate the diverted plasma, boundary islands, and the scrape-off layer (SOL), respectively. Purple lines indicate in-vessel components of divertor and baffle plates.
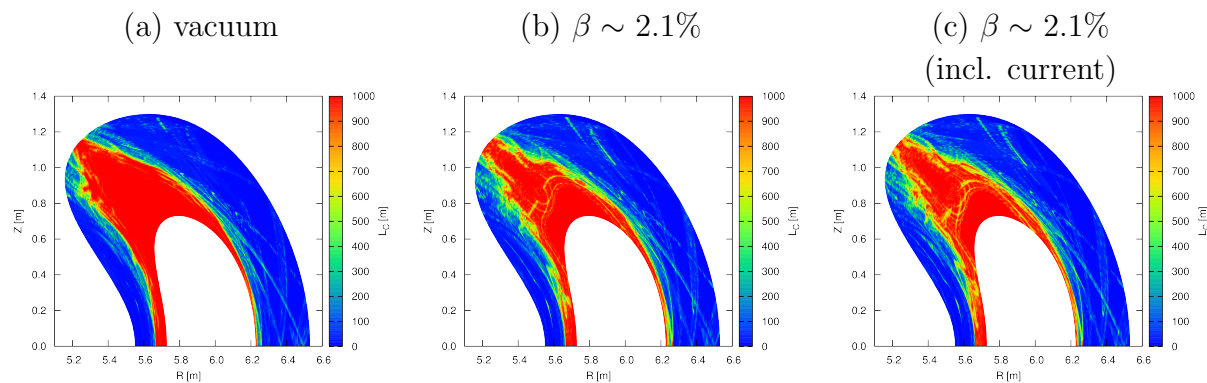
(a) vacuum   (b) $\beta \sim 2.1\%$ (c) $\beta \sim 2.1\%$
                                                    (incl. current)

Figure 5. Contours of the connection length of the magnetic field line for 3D MHD equilibria are shonw for the medium density case in a case of the beta effect only and another case including both effects of the plasma beta and toroidal current. For a comparison, the vacuum field is also shown. Contours are plotted at the bean-shaped cross section.
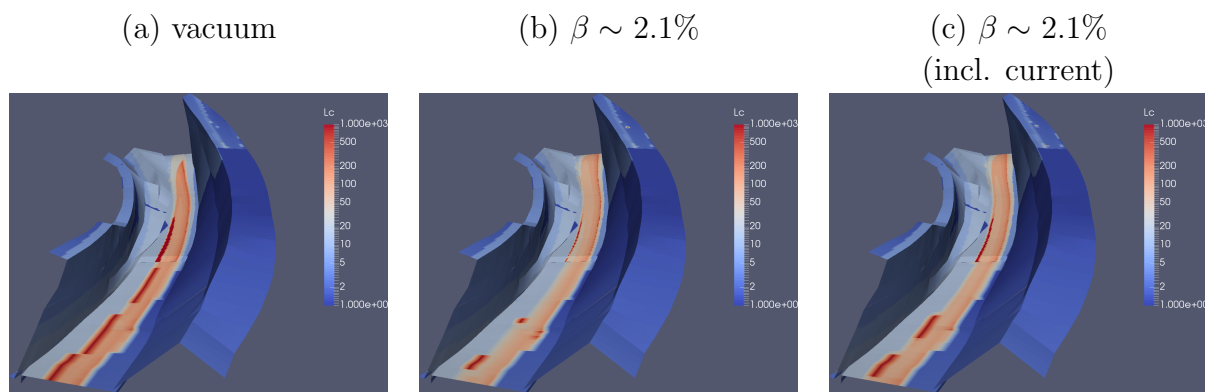
(a) vacuum (b) $\beta \sim 2.1\%$ (c) $\beta \sim 2.1\%$ (incl. current)

Figure 6. Patterns of the footprint on in-vessel components for 3D MHD equilibria are shonw for the medium density case in a case of the beta effect only and another case including both effects of the plasma beta and toroidal current. For a comparison, the vacuum field is also shown. The footprint is calculated on divertor and baffle plates install to the bottom of the device. The bird's eye view of the footprint is shown.
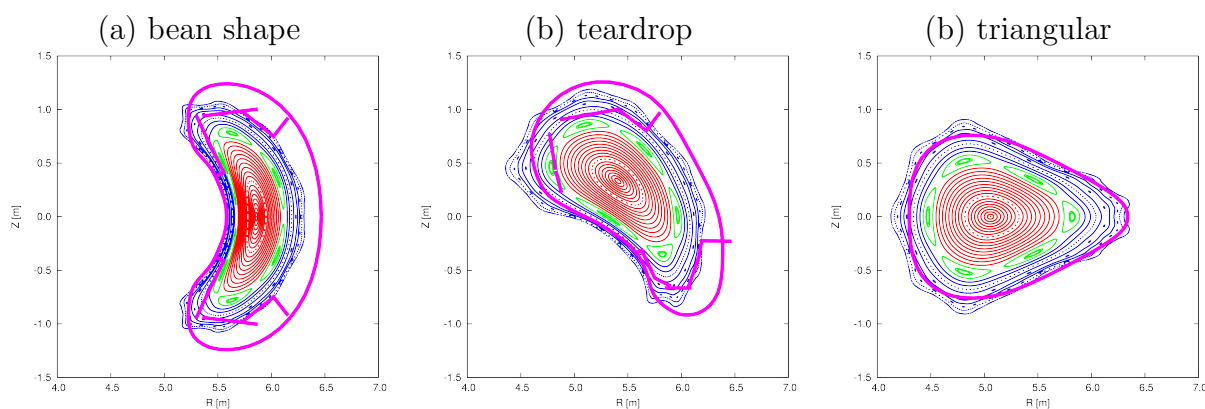
(a) bean shape (b) teardrop (b) triangular

Figure 7. Poincaré plots of the low-iota configuration are shown for the vacuum field. The boundary iota is 5/6. Three poloidal cross section are plotted corresponding to figure 1.
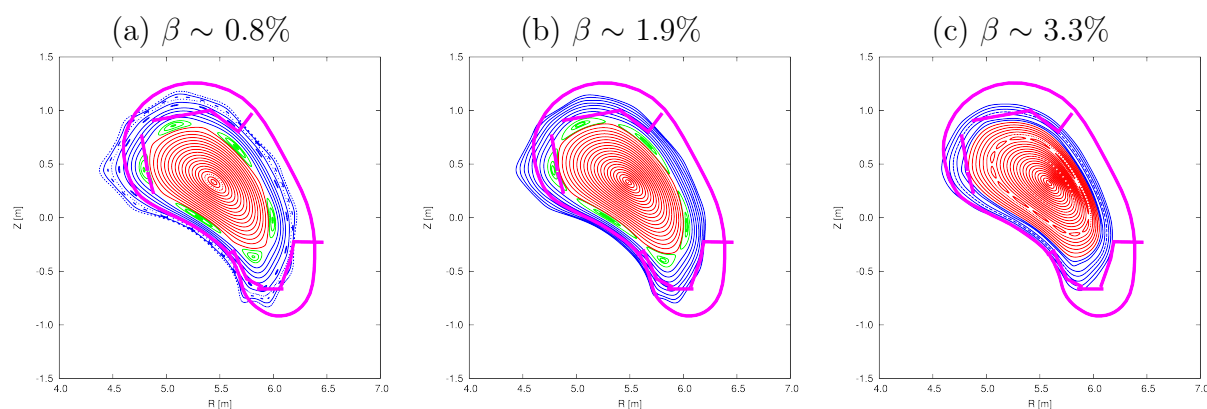
Figure 8. 3D MHD equilibria for the low ,medium, and high density cases are shown at the teardrop cross section. Results are shown for a case of the beta effect only. For a comparison, the vacuum field is also shown. Red dots, green dots, and blue dots indicate the diverted plasma, boundary islands, and the scrape-off layer (SOL), respectively. Purple lines indicate in-vessel components of divertor and baffle plates.
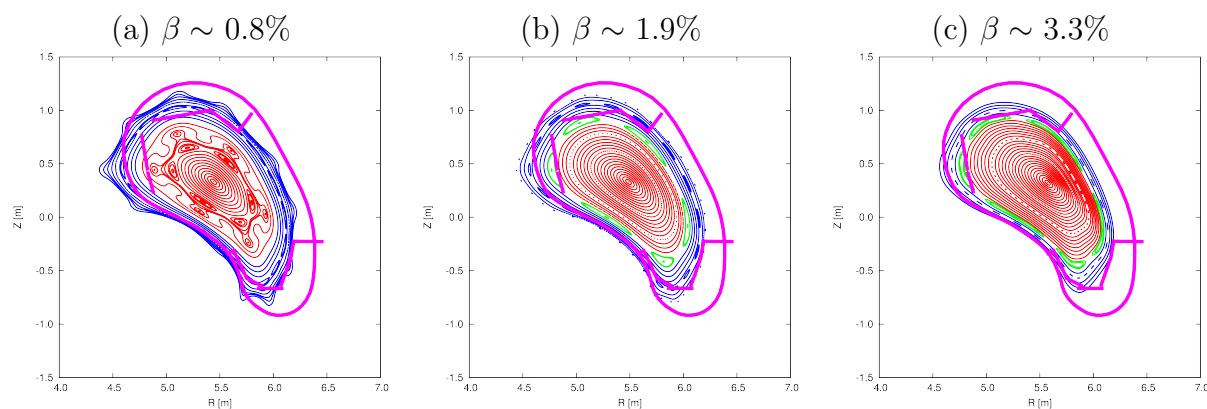

Figure 9. 3D MHD equilibria for the low ,medium, and high density cases including the toroidal current density are shown at the teardrop cross section. Results are shown for a case of the beta effect only. For a comparison, the vacuum field is also shown. Red dots, green dots, and blue dots indicate the diverted plasma, boundary islands, and the scrape-off layer (SOL), respectively. Purple lines indicate in-vessel components of divertor and baffle plates.